International Journal of Nanomedicine

Dovepress
Taylor & Francis Group

Open Access Full Text Article

ORIGINAL RESEARCH

An Experimental Study into the Photodynamic/Sonodynamic Therapy of Triple-Negative Breast Cancer Mediated by the Novel Nano-Photonic Sensitizer NBDPBr Nanoparticles

Qian Huang[1], Leichen Wang[2], Yaqi Zhang[1], Lilin Zhao[1], Ting Zhang[1]

[1]Department of Ultrasound, The Affiliated Cancer Hospital of Nanjing Medical University, Jiangsu Cancer Hospital, Jiangsu Institute of Cancer Research, Nanjing, Jiangsu, 210009, People's Republic of China; [2]Key Laboratory of Flexible Electronics (KLOFE) & Institute of Advanced Materials (IAM), Nanjing Tech University (NanjingTech), Nanjing, Jiangsu, 211800, People's Republic of China

Correspondence: Ting Zhang, Email zhangting@jszlyy.com.cn

Purpose: This study aimed to develop a synergistic photodynamic therapy/sonodynamic therapy (PDT/SDT) system that utilises novel NBDPBr nanoparticles (NPs). These NBDPBr NPs are composed of the aza-boron-dipyrromethene (Aza-BODIPY) dye NBDPBr, which is encapsulated in amphiphilic polymer F-127 (Pluronic®). The system is intended for the treatment of triple-negative breast cancer (TNBC), and simultaneously establishes a multimodal imaging platform for real-time monitoring of the therapeutic effect.

Methods: The photophysical properties of the NBDPBr NPs were characterised. Singlet oxygen ($^1O_2$) generation was assessed under laser (L) and ultrasound (US) irradiation. In vitro cytotoxicity and reactive oxygen species (ROS) production were evaluated in 4T1 TNBC cells. The therapeutic effect and biosafety in vivo were tested by using a syngeneic TNBC mouse model, and it was monitored by ultra-resolution micro-imaging (URM) and photoacoustic imaging (PAI).

Results: The spherical NBDPBr NPs showed excellent stability, with an average diameter of about 82.9 nm. Combined laser and ultrasound irradiation induced the highest $^1O_2$ production, leading to 96.02% cell death in vitro and near-complete tumor suppression in vivo, with no significant systemic toxicity. URM revealed decreased tumor microvascular density and PAI indicated reduced blood oxygen saturation post-treatment, confirming synergistic PDT/SDT-induced vascular disruption and tumor hypoxia.

Conclusion: NBDPBr NPs mediate potent synergistic PDT/SDT against TNBC, supported by a dual-modal URM/PAI imaging platform for treatment monitoring. This study presents a promising theranostic strategy with high translational potential for TNBC management.

Keywords: photosensitizers, nanoparticle, photodynamic therapy, sonodynamic therapy, triple-negative breast cancer, multimodal imaging, synergistic therapy

Introduction

Breast cancer is the most commonly diagnosed malignancy among women worldwide, which seriously endangers health and survival.[1] Among its subtypes, triple-negative breast cancer (TNBC) is particularly aggressive and difficult to treat due to the absence of estrogen receptor, progesterone receptor, and HER2 expression, which limits targeted therapeutic options.[2]

Photodynamic therapy (PDT) and sonodynamic therapy (SDT) are emerging as promising non-invasive modalities for cancer treatment. Both rely on the activation of a sensitizer by external energy (light or ultrasound) to generate cytotoxic reactive oxygen species (ROS), primarily singlet oxygen ($^1O_2$), within tumor tissue.[3] They demonstrate advantages such as high targeting accuracy and non-invasiveness. However, the efficacy of single-modality therapies is limited due to tumor heterogeneity.[4] Although PDT has excellent spatial selectivity,[5] its effectiveness is limited to the shallow penetration of light and is ineffective for deep tumors. In contrast, SDT can produce ROS even in deeper tissues thanks to the superior penetration of ultrasound in tissues.[6] Therefore, the combination of PDT and SDT could overcome their respective limitations and provide a more effective way to treat solid tumors, especially those deep in the tissue or with heterogeneity.

https://doi.org/10.2147/IJN.S576927
Received: 14 November 2025
Accepted: 12 March 2026
Published: 28 March 2026

Real-time imaging guidance is crucial for monitoring the treatment response and optimizing the therapeutic effect. Ultra-resolution micro-imaging (URM) can achieve high-resolution visualization of tumor microvessels by tracking contrast microbubbles, so as to dynamically evaluate vascular changes.[7] Photoacoustic imaging (PAI) combines the high contrast of optical imaging with the deep penetration of ultrasound, which can quantitatively monitor the oxygen saturation of tumor.[8] The integration of URM and PAI provides a comprehensive platform for assessing structural (vascular) and functional (oxygenation) changes during treatment.

Aza-boron-dipyrromethene (Aza-BODIPY) dyes are attractive as photosensitizers because of their adjustable optical properties, high molar extinction coefficients in the near-infrared (NIR) region and excellent photostability. It has been widely used in optical imaging and tumor diagnosis.[9] Heav-atom (eg, bromine) substitution on the Aza-BODIPY core can significantly promote intersystem crossing (ISC), thus enhancing the generation of $^1O_2$ —a critical process for both PDT and SDT efficacy.

In our previous work, we synthesized a new type of dibrominated Aza-BODIPY derivative, NBDPBr, which had a high singlet oxygen quantum yield ($\Phi\Delta$ = 66%) and a significant photothermal conversion efficiency (43.0%), showing its potential as a phototherapy dual-function agent.[10] However, its sonodynamic activity and the potential of photoacoustic activation combined therapy have not been explored.

Based on our previous research, this study systematically solves the limitations of single-modal phototherapy through three key advances. First of all, we evaluated the sonodynamic activity of NBDPBr for the first time, thus establishing it as a dual-energy responsive sensitizer that can be activated by 660 nm laser and ultrasound at the same time. Secondly, we clarified the synergistic mechanism of this combination and proved that the sequential irradiation of laser and ultrasound would trigger a coordinated active ROS generation process, and the $^1O_2$ level produced was significantly higher than that of any stimulation alone. Third, we have promoted the integrated method of diagnosis and treatment by combining the synergy of PDT/SDT with the dual-modal imaging platform of URM and PAI. The platform can visualize the vascular destruction and hypoxia caused by treatment in real time, and provide direct functional feedback for the treatment effect.

The encapsulation of NBDPBr within amphiphilic polymer F-127 (NBDPBr NPs) increases its water solubility and colloidal stability, as well as its accumulation in tumours through the enhanced permeability and retention effect. The bromine atoms on the aryl rings not only elevate the singlet-oxygen quantum yield for PDT but also promote electron-transfer processes under ultrasound, rendering NBDPBr structurally advantageous for synergistic energy conversion under both optical and acoustic stimulation.

Therefore, this study aims to systematically evaluate a novel nano-theranostic system that integrates dual-mode energy-activated therapy (PDT/SDT) with dual-mode imaging monitoring (URM/PAI), as outlined in Scheme 1. We seek to establish a preliminary preclinical foundation for a more comprehensive and image-guided strategy against TNBC.

Materials and Methods

Materials

Chemicals and Reagents

Aza-BODIPY derivative NBDPBr, Pluronic® F-127 (Sigma-Aldrich®, Shanghai, China), PBS, isoflurane, SonoVue microbubble contrast agent (Bracco, Italy).

Instruments

Transmission electron microscope (TEM, JEOL JEM-2100 electron microscope, accelerating voltage: 200 KV), Dynamic light scattering (DLS) analyzer (Micromeritics Nanoplus-3 (US) system), Ultrasonic cleaner (for nanoparticle preparation, SB-4200D, SCIENTZ, Ningbo, China), 660 nm laser (Changchun Leishe MW-GX-660), UV-vis-NIR spectrophotometer (UV-3600, Shimadzu, Japan), ultrasound therapy device (DM-200F, Dimip, Shenzhen, China), Diagnostic and Therapeutic Ultrasound System (VINNO9E, VINNO Technology, Suzhou, China), photoacoustic imaging system (Resona Y, Mindray, China).

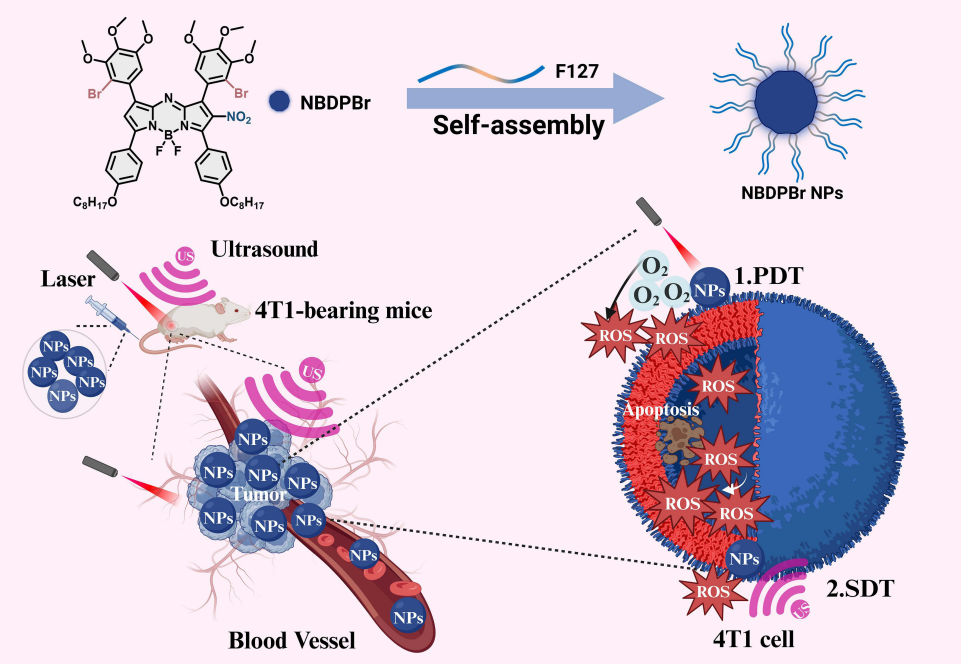

Scheme 1 Illustration for the preparation of NBDPBr NPs and photodynamic /sonodynamic therapy mechanism. Created with BioRender.com. 1. PDT represents the photodynamic therapy process, in which the NBDPBr NPs are activated by 660 nm laser irradiation to generate reactive oxygen species (ROS); 2. SDT represents the sonodynamic therapy process, in which the NBDPBr NPs are activated by ultrasound irradiation to produce ROS.

Cell Lines and Animals

4T1 TNBC cells, HeLa (human cervical adenocarcinoma) cells, and HUVECs (Human Umbilical Vein Endothelial Cells) were purchased from the Institute of Biochemistry and Cell Biology, SIBS, CAS (China). To assess the broad-spectrum antitumor potential and selective cytotoxicity of NBDPBr NPs, two additional cell lines were employed: HeLa cells, serving as a model of non-TNBC epithelial cancer, and HUVEC, serving as a model of normal vascular endothelial cells. Female BALB/c mice, aged 6–8 weeks, were procured from GemPharmatech Co., Ltd. (Jiangsu, China) and maintained under specific-pathogen-free (SPF) conditions within a barrier facility. The facility was regulated for temperature and humidity and operated on a 12-hour light/dark cycle. The mice were provided with ad libitum access to sterilized food and water and were acclimatized for a minimum of one week prior to the commencement of experiments. The animal use license for this study was SYXK (Su) 2023–0029. All experimental procedures involving animals received approval from the Ethics Committee of Nanjing Medical University (Approval No. 2504063) and were conducted in accordance with Chinese national guidelines for the care and use of laboratory animals, the American Veterinary Medical Association (AVMA) Guidelines for the Euthanasia of Animals, and the Guide for the Care and Use of Laboratory Animals.

Animal Welfare and Ethical Measures

To minimize animal suffering, predefined humane endpoints were established in accordance with the NC3Rs guidelines on Humane Endpoints. The criteria included: (1) a weight loss exceeding 20% of the baseline body weight; (2) a tumor volume exceeding 10% of body weight or the presence of ulceration or infection; (3) an inability to voluntarily consume food or water; and (4) manifestations of severe lethargy or distress. The well-being of the animals was assessed at least twice daily, and any mouse that reached these endpoints was euthanized immediately.

Anesthesia and Euthanasia

For procedures necessitating anesthesia, mice were anesthetized using inhaled isoflurane, with induction at a concentration of 2.5% and maintenance at 1.8%, administered through a precision vaporizer with 100% oxygen at a flow rate of 2 L/min. The depth of anesthesia was monitored by evaluating the respiratory rate and the pedal withdrawal

https://doi.org/10.2147/IJN.S576927

reflex. At the conclusion of the experiment, mice were deeply anesthetized with an overdose of isoflurane, followed by euthanasia through cervical dislocation. The absence of spontaneous respiration and heartbeat was used to confirm death.

Preparation and Characterization of NBDPBr NPs

The target aza-BODIPY derivative NBDPBr was synthesized via a multi-step route according to our previous work.[10] The synthesis commenced with the formation of a chalcone intermediate via an aldol condensation. A Michael addition with nitromethane then afforded a nitro-functionalized precursor in moderate yield. Subsequent reflux in the presence of ammonium acetate facilitated cyclization to form the pivotal pyrrole moiety. Complexation with boron trifluoride yielded the core aza-BODIPY fluorophore. This core was then nitrated in nitric acid at 0 °C to furnish the nitro-substituted compound. Finally, bromination was achieved using N-bromosuccinimide (NBS) as the bromination agent to give the final target molecule.

NBDPBr (1 mg) and amphiphilic polymer F-127 (10 mg) were vigorously mixed in tetrahydrofuran (1 mL) using an ultrasonic cleaner operating at a frequency of 40 kHz and a power of 480 W for 15 minutes to form a homogeneous mixture. The heterogeneous solution was swiftly injected into deionized water under turbulent agitation. During the rapid solvent evaporation, intermittent stirring at room temperature yielded a uniform dispersion. Ultrafiltration through a 220 nm membrane afforded pure NBDPBr NPs devoid of aggregates or impurities. Transmission electron microscopy revealed their well-defined shapes and sizes, while dynamic light scattering quantified their hydrodynamic diameters in situ. UV-vis absorbance spectrum of NBDPBr NPs was recorded with a UV-3600 Shimadzu UV-vis-NIR spectrometer.

ROS Generation Assay

$^1O_2$ generation was quantified using 1,3-diphenylisobenzofuran (DPBF) as a probe, monitoring absorbance decay at 415 nm.

Photodynamic Detection

Experiments were performed to quantify $^1O_2$ production. Specifically, a detection solution was prepared with DPBF and NBDPBr NPs at a concentration of 20 μg/mL. The sample was then irradiated with a 660 nm laser with an intensity of 0.1 W/cm^2. Absorption spectra were collected every 20s as the experiment progressed. By monitoring the decrease in absorbance at 415 nm over time, the decomposition rate of DPBF could be determined to characterize the production of $^1O_2$.

Acoustic Detection

A detection solution containing DPBF and NBDPBr NPs (20 μg/mL) was prepared. To establish the baseline for ROS generation by the nanoparticles themselves, the NBDPBr NPs only (Control) group was kept in the dark without any laser or ultrasound irradiation. For the NBDPBr NPs + US group, ultrasonic treatment (1.0 W/cm^2, 40% duty cycle) was applied, with absorption spectra collected every minute after each treatment. The NBDPBr NPs + L + US group received 20s of 660 nm laser irradiation (0.1 W/cm^2), followed by ultrasonic treatment (1.0 W/cm^2, 40% duty cycle). Absorption spectra were recorded after each treatment to assess the absorbance decrease at 415 nm, calculate the DPBF decomposition rate, and characterize oxygen production.

In vitro Experiments

Cell Culture

4T1 and HeLa cells were cultured in RPMI-1640 medium containing 10% fetal bovine serum (FBS) and 1% penicillin-streptomycin. HUVECs were cultured in endothelial cell growth medium (ECM) supplemented with 10% FBS, 1% penicillin-streptomycin, and endothelial cell growth factors. All cell lines were maintained in a humidified incubator at 37°C with 5% CO_2. Cells were routinely cultured in 25 cm^2 culture flasks and passaged upon reaching 70–80% confluence using 0.25% trypsin-EDTA. All cell culture procedures were carried out under aseptic conditions in a laminar flow hood to maintain sterility. Cells utilized in the experiments were within 10 passages after resuscitation to ensure phenotypic consistency.

Experimental Setup

Inoculate 4T1, HeLa and HUVEC cells in a 96-well plate with a density of about 1×10^4 cells per well, and let them stick to the wall overnight. The addition of HUVEC cells aims to evaluate the potential toxicity of NBDPBr NPs to normal vascular cells, while HeLa cells are used to test their efficacy on cells other than TNBC. The next day, the culture medium was replaced with a fresh medium containing 40 μg/mL NBDPBr NPs, or the culture medium without NPs as the control group. After 4 hours of co-incubation, the cells were processed according to the grouping situation. After incubation, the cells were divided into five groups: control, NBDPBr NPs only, NBDPBr NPs + L, NBDPBr NPs + US and NBDPBr NPs + L + US. Each group is subjected to specific treatment, including laser irradiation (wavelength 660 nm, intensity 0.8 W/cm^2 for five minutes) and ultrasound treatment (intensity 1.0 W/cm^2, a 40% duty cycle lasting three minutes).

Cytotoxicity Assay

In order to quantitatively evaluate cell viability under different treatment conditions, the MTT detection method is adopted. After the corresponding treatment of each experiment, the cells were further cultured for 12 hours. Then, add 20 μL of MTT solution (5 mg/mL in PBS) to each well and incubate at 37°C for 4 hours. The formed methylene crystals are then dissolved with 200 μL of dimethylsulfoxide (DMSO). Use an enzyme marker to measure the absorbance of each well at 492 nm. The cell viability was calculated as a percentage relative to the control group. Each experiment should be repeated independently at least three times. At the same time, the survival and death status of cells was qualitatively analyzed using the live/dead viability/cytotoxicity assay of living/dead cells. After treatment, the cells were washed with PBS and co-stained with 2 μM Calcein-AM and 4 μM propidium iodide (PI) for 20 minutes at 37°C in the dark. Viable cells, which have intact membranes, metabolize Calcein-AM to produce a uniform green fluorescence, indicating living cells. In contrast, PI enters only cells with compromised membranes, staining the nuclei of dead cells red. Fluorescence images were acquired using an inverted fluorescence microscope.

Detection of ROS

Intracellular ROS levels were assessed using the DCFH-DA fluorescent probe. After treating cells under different conditions, DCFH-DA dye was added and incubated for 30 minutes. The intensity of green fluorescence was observed through an inverted fluorescence microscope. Green fluorescence indicates ROS production within the cell.

In vivo Experiments

A group of 6-8-week-old female BALB/c nude mice was selected for the study. Each mouse had 5×10^5 4T1 breast cancer cells implanted subcutaneously into their right hind limb. The researchers observed tumor growth every couple of days and started the experiment once the tumors reached approximately 100 mm^3.

Experimental Setup

BALB/c nude mice were randomly divided into six groups (n=5): control, NBDPBr NPs only, L + U, NBDPBr NPs + L, NBDPBr NPs + US, and NBDPBr NPs + L + US. Mice in the treatment groups received NBDPBr NPs solution (300 μg/mL) via tail vein injection, with the injection volume calculated based on body weight (3 mg/kg). After 7–9 hours, tumors were irradiated with laser and/or ultrasound according to group assignment, using the same parameters as the in vitro experiments. Ultrasound irradiation was performed using the Demai DM-200F ultrasonic therapy device.

Tumor Growth Monitoring

Throughout the 16-day treatment, the tumor's longest (a) and shortest (b) diameters were measured with calipers every 2 days, the tumor volume was calculated ($V = a \times b^2/2$), and the tumor growth curve of each group was recorded to determine the antitumor effect of different treatments.

Ultrasound Imaging Monitoring

1. URM: Using a VINNO ultrasound system with a high-frequency U5-15L probe, tumor imaging was conducted before and after treatment. Mice were anesthetized with isoflurane, and a 0.1 mL contrast agent was injected via the tail vein. URM was used to observe microvascular structural changes and assess treatment effects on tumor

angiogenesis. 2. PAI: Additionally, a Mindray photoacoustic imaging system with an L9-3PAU probe analyzed tumor tissue at 750 nm and 830 nm wavelengths to measure blood oxygen saturation (sO_2). Photoacoustic signals were generated to quantitatively analyze oxygenated hemoglobin (HbO_2) and deoxygenated hemoglobin (Hb), thereby obtaining tumor tissue sO_2:

$$sO_2 = \frac{HbO_2}{HbO_2 + Hb}$$

The effect of the therapy on tumor oxygenation was evaluated by comparing the changes of sO_2 between treatment groups.

Biosafety Evaluation

After the experiment, the mice were weighed to monitor the weight changes; the main organs (heart, liver, spleen, lungs and kidneys) were examined histologically to assess the biosafety of NBDPBr NPs.

Histological Examination

After euthanasia, removed the tumor tissue and organs, fixed them with 4% polyformaldehyde, paraffin-embedded, and sectioned. Morphological changes were evaluated through H&E staining, and TUNEL staining identified cell apoptosis in tumor tissues. Examine the sample with a microscope and take photos for analysis.

Statistical Analysis

Data were analyzed using GraphPad Prism 10 and presented as mean ± standard deviation (SD). One-way ANOVA was used for the comparison between multiple groups, followed by the Tukey's post-test, while the LSD-*t* test was applied for two-group comparisons. $P<0.05$ was considered statistically significant.

Results

Characterization of NBDPBr NPs

TEM observations (Figure 1a) shows that the NBDPBr NPs prepared by nanoprecipitation are uniformly spherical, with a diameter of about 80 nm. The measurement results of dynamic light scattering (DLS) confirm these findings, indicating that its average hydrodynamic size is about 82.9 nm, and the polydispersity index (PDI) is as low as 0.176 (Figure 1b), indicating that its dispersion and stability are good, which is conducive to improving tumor penetration and retention. In addition, by monitoring the hydrodynamic diameter of NBDPBr NPs within a week, its colloidal stability was confirmed, and its diameter remained basically unchanged (Figure 1c). The Zeta potential of these NBDPBr NPs is about −5.45 mV, indicating that their surface has a certain negative charge, which contributes to the stability of the colloid through electrostatic rejection.

UV-Vis-NIR spectrometer analysis (Figure 1d) shows that there is a strong absorption peak at 640 nm, highlighting their excellent near-infrared light capture ability, making them an ideal choice for photodynamic therapy in deep tissues. In addition, the morphology of NBDPBr NPs is uniform and the monodispersity is good, which shows the great potential of this nanoplatform in clinical transformation. The results collectively indicate that the as-prepared NBDPBr NPs could serve as a versatile nanoplatform for enhanced photodynamic cancer therapy.

Ability of NBDPBr NPs to Generate ($^1O_2$)

The $^1O_2$ generation capacity of NBDPBr NPs was assessed by DPBF probe under laser (L), ultrasound (US), and combined (L+US) irradiation.

As shown in Figure 2a, the absorbance of DPBF at 415 nm decreased rapidly upon laser irradiation in the presence of NBDPBr NPs. Correspondingly, Figure 2b showed a statistically significant increase ($P<0.001$) in $^1O_2$ production after 20s of laser exposure, demonstrating substantial $^1O_2$ production by NBDPBr NPs.

While sono-dynamic therapeutics with NBDPBr NPs showed higher $^1O_2$ levels over longer periods of ultrasound, the combined approach of preliminary laser irradiation substantially augmented photo-oxygenation (Figure 2c). From just three minutes following the dual treatment, NBDPBr NPs activated by both light and sound generated significantly

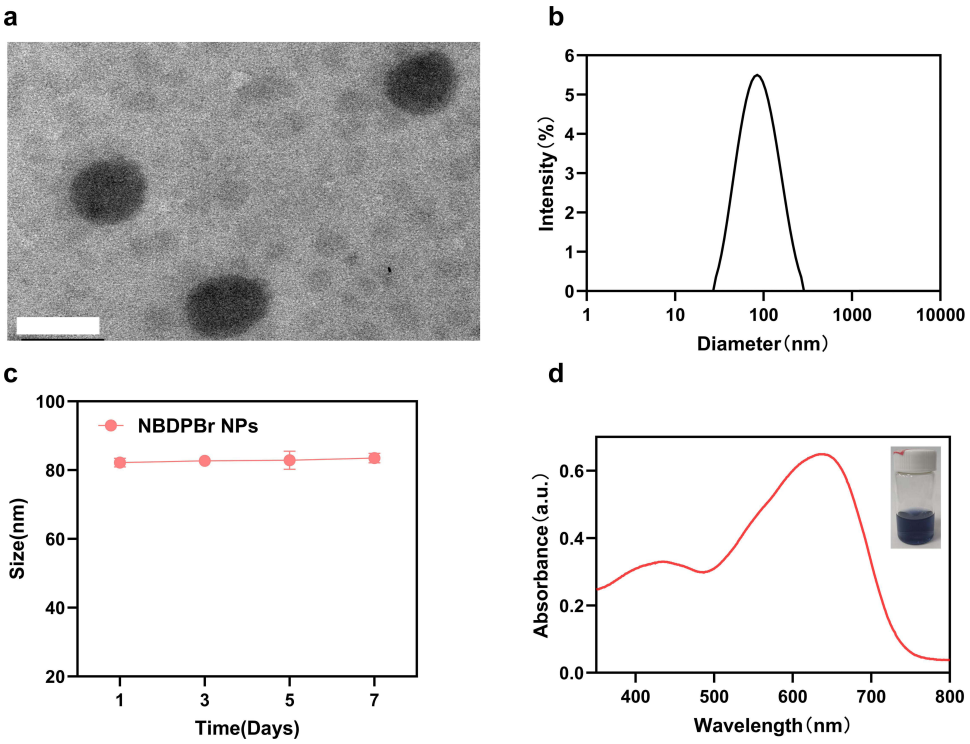

Figure 1 Characterization of NBDPBr NPs. (**a**) TEM image of NBDPBr NPs, scale bar: 100 nm; (**b**) DLS size distribution of NBDPBr NPs; (**c**) Hydrodynamic diameter variations of NBDPBr NPs over a week (n = 3); (**d**) UV-Vis absorption spectrum of NBDPBr NPs in aqueous solution.

greater $^1O_2$ than ultrasound alone, as evidenced by statistical analysis. This dual synergy demonstrates the capacity of laser and ultrasound to separately produce $^1O_2$ from the NPs, with a cooperative effect exceeding either modality when applied in tandem. The combined method thus capitalizes on the photoacoustic abilities of each energy source to maximize therapeutic oxidative stress at the target site.

Results of in vitro Experiments

Cytotoxicity Assessment

In the MTT experiment (Figure 3a and b), laser, ultrasonic irradiation, and NBDPBr NPs demonstrated good biocompatibility with 4T1cells and HUVEC, showing over 90% cell survival and no significant cytotoxicity or cell damage.

As shown in Figure 3c, NBDPBr NPs mediated significant cytotoxicity upon activation. The cell death rates for the NBDPBr NPs+US and NBDPBr NPs+L groups were 64.01% and 71.51%, respectively. Strikingly, the combined NBDPBr NPs+L+US treatment achieved 96.02% cell death in 4T1 cells, significantly outperforming all other groups ($p < 0.001$). This potent effect was also observed in HeLa cells (Figure 3d), suggesting broad-spectrum antitumor potential.

These revelations propose that NBDPBr NPs are effective in killing cancer cells under laser and ultrasound excitation, with the integrated therapy being most powerful. This confirms that the synergy between PDT and SDT has extraordinary therapeutic effects.

Detection of Live/Dead-Cell Staining

Live cell staining (Figure 3e) showed that NBDPBr NPs were non-toxic without laser or ultrasound, which can be seen from mainly green fluorescent cells. When laser or ultrasound is used alone, the cell vitality decreases slightly, manifested as an increase in red fluorescence. However, when NBDPBr NPs are combined with laser and ultrasound, strong red fluorescence fills the entire field of vision, indicating significant cell death, which is consistent with the MTT test results, which confirms the effectiveness of combined therapy in killing tumor cells.

https://doi.org/10.2147/IJN.S576927

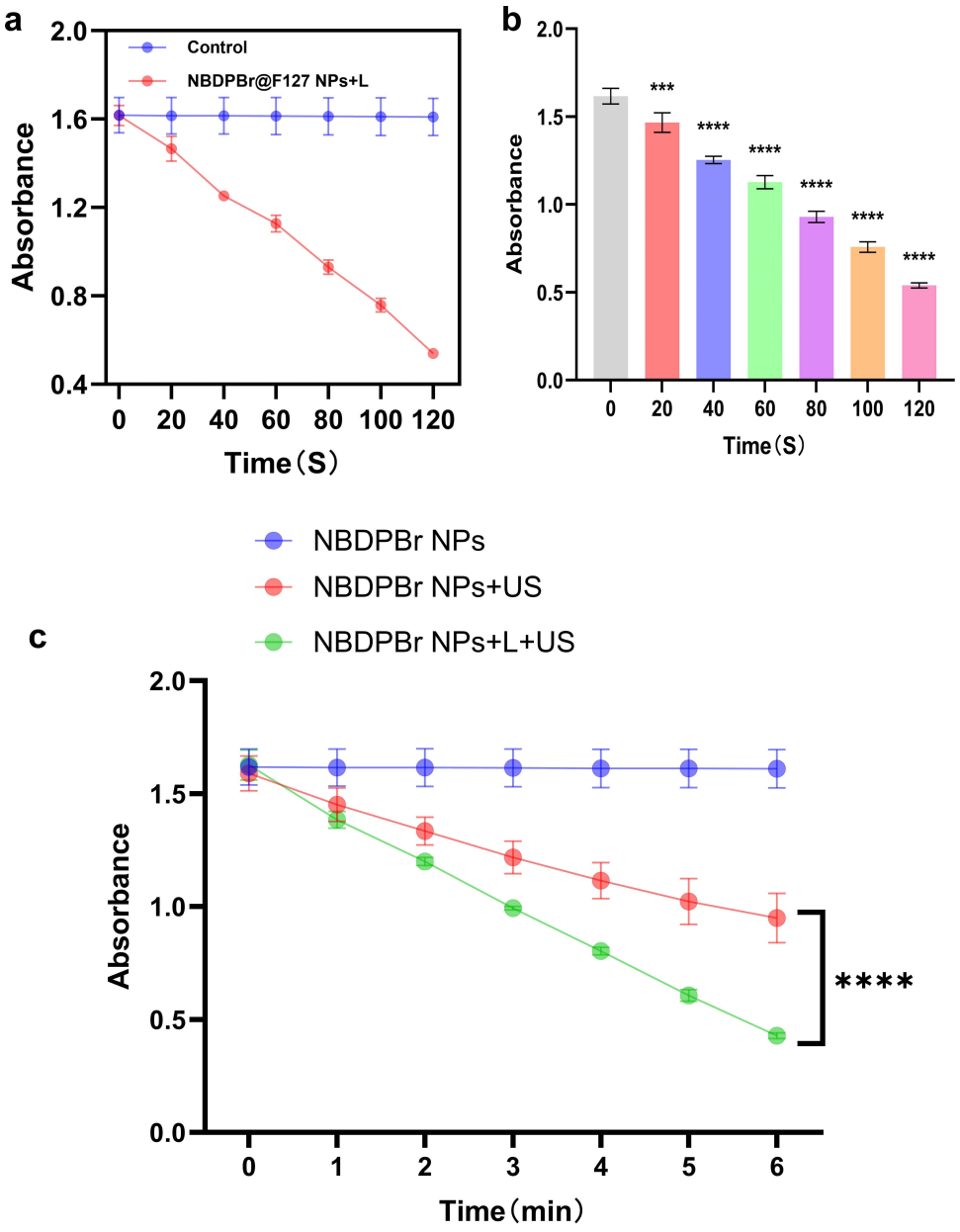

Figure 2 NBDPBr NPs photodynamic and acoustic dynamic effect. (**a**) Absorbance change of DPBF at 415 nm; (**b**) Absorbance change of $^1O_2$ probe DPBF in NBDPBr NPs solution under illumination at different times. (***P <0.001, ****P <0.0001, compared with the control group at 0s); (**c**) Singlet oxygen ($^1O_2$) generation in NBDPBr NPs solution under different ultrasound conditions. The NBDPBr NPs+US group received ultrasound therapy (1.0 W/cm^2, 40% duty cycle) for 6 min, while the NBDPBr NPs+L +US group first underwent 660 nm laser irradiation (0.1 W/cm^2) for 20s before receiving ultrasound treatment for 6 min. (* indicates statistically significant difference between the specified groups; ****P <0.0001; n=3).

Detection of Intracellular ROS Generation

DCFH-DA fluorescent probe was used to determine the level of reactive oxygen in cells. As shown in Figure 3f, compared with the control group and the NBDPBr NPs group, the NBDPBr NPs + L group and the NBDPBr NPs + US group emitted green fluorescence. The NBDPBr NPs + L + US group showed strong green fluorescence, indicating that the production of reactive oxygen was significant. This suggests that NBDPBr NPs can effectively enhance reactive oxygen species generation through the combined application of laser and ultrasound, leading to cellular oxidative damage and apoptosis.

https://doi.org/10.2147/IJN.S576927

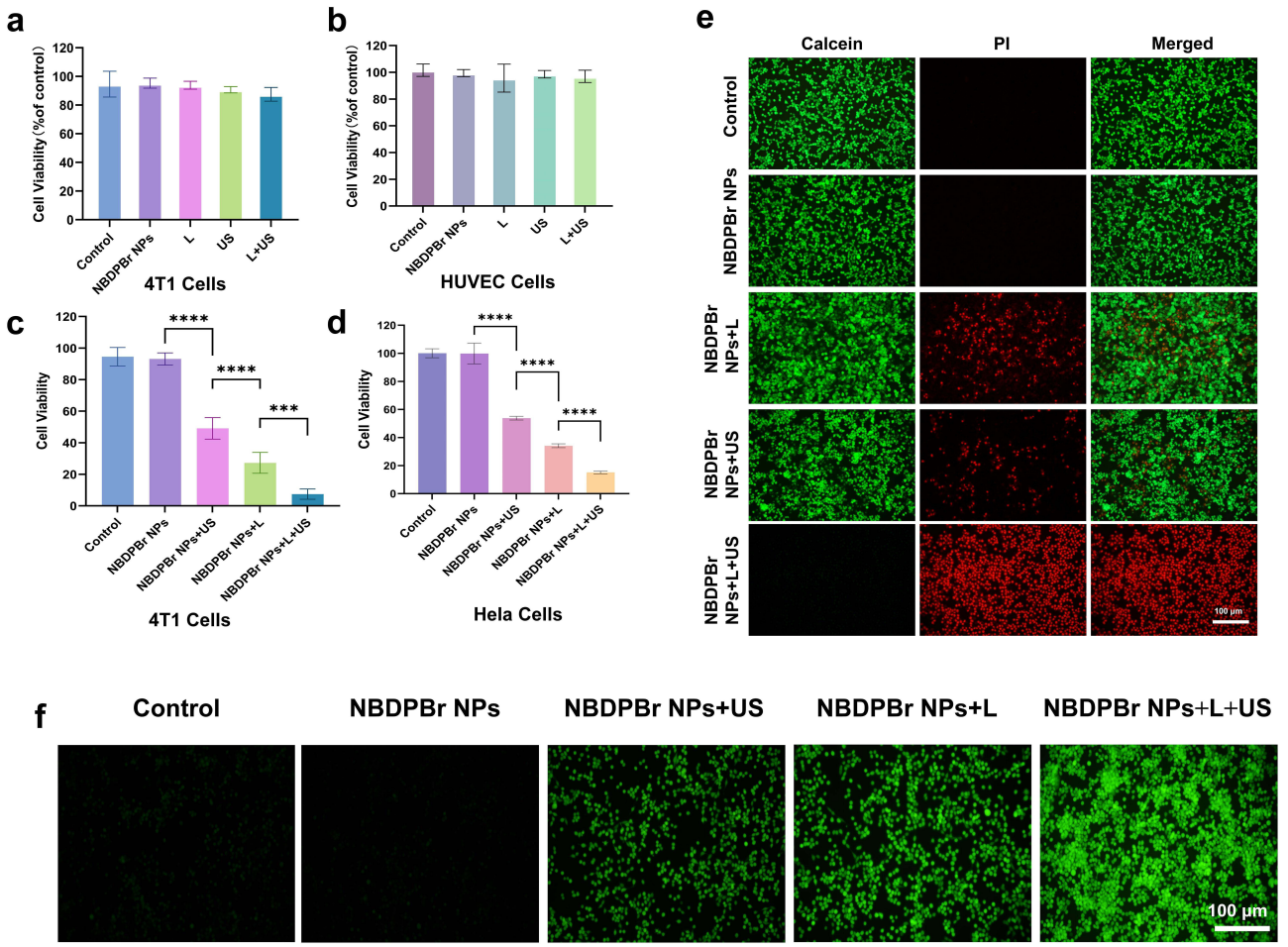

Figure 3 In vitro evaluation of biocompatibility, cytotoxicity, and therapeutic mechanism of NBDPBr NPs. (**a**) Group L received 660 nm laser irradiation (power 0.8 W/cm^2) for 5 min, and Group US received ultrasonic treatment (power 1.0 W/cm^2, duty cycle 40%) for 3 min. Group L+US first received 660 nm laser irradiation (power 0.8 W/cm^2) for 5 min, and then received ultrasonic irradiation (power 1.0 W/cm^2, duty cycle 40%) for 3 min; (**b**) Biocompatibility assessment on HUVECs; (**c**) Following the co-incubation of NBDPBr NPs with 4T1 cells, along with exposure to laser and ultrasound irradiation under varying conditions, the viability of the 4T1 cells was assessed using the MTT assay. (* indicates statistically significant difference between the specified groups; *** indicating $P < 0.001$; **** indicating $P < 0.0001$; n = 3); (**d**) Cytotoxicity of NBDPBr NPs mediated treatments against HeLa cells (a non-TNBC epithelial cancer model); (**e**) 4T1 cells staining by calcein-AM/propidium iodide (PI) with green fluorescence (excitation wavelength 455 nm, live cells) or red fluorescence (excitation wavelength 560 nm, dead cells), scale bar = 100 μm; (**f**) Except for the Control group, 4T1 cells were co-incubated with NBDPBr NPs for 4 hours, and then DCFH-DA was added to stain ROS. Green fluorescence represented DCF (excitation wavelength 455 nm), reflecting the intracellular ROS level. Scale bar = 100 μm.

Results of in vivo Experiments

Tumor Growth Monitoring

In in vivo anti-tumor experiments, tumor-bearing nude mice were divided into six treatment groups. Figure 4a shows that the L + US and only NBDPBr NPs injection groups experienced rapid tumor growth similar to the control group. In contrast, the combined treatment groups (NBDPBr NPs + L, NBDPBr NPs + US) showed reduced tumor growth. The most effective was the photoacoustic combined therapy (NBDPBr NPs + L + US), which nearly halted tumor growth with significant differences from the control group ($P < 0.05$), indicating its potential to inhibit triple-negative breast cancer.

URM

Before treatment, tumor tissues showed uneven microvessel distribution. Post-treatment, microvascular structures and blood flow changed. As Figure 4b demonstrates, microvascular density increased in the control and NBDPBr NPs groups, indicating tumor angiogenesis. On the contrary, the microvessels and blood flow of the combined therapy group (NBDPBr NPs + L + U) were significantly reduced, indicating that angiogenesis was inhibited and blood supply was reduced.

Table 1 summarizes the quantitative analysis of microvascular density before and after treatment. There was no statistically significant difference in the baseline microvascular density of each group before treatment ($P = 0.075$), which

https://doi.org/10.2147/IJN.S576927

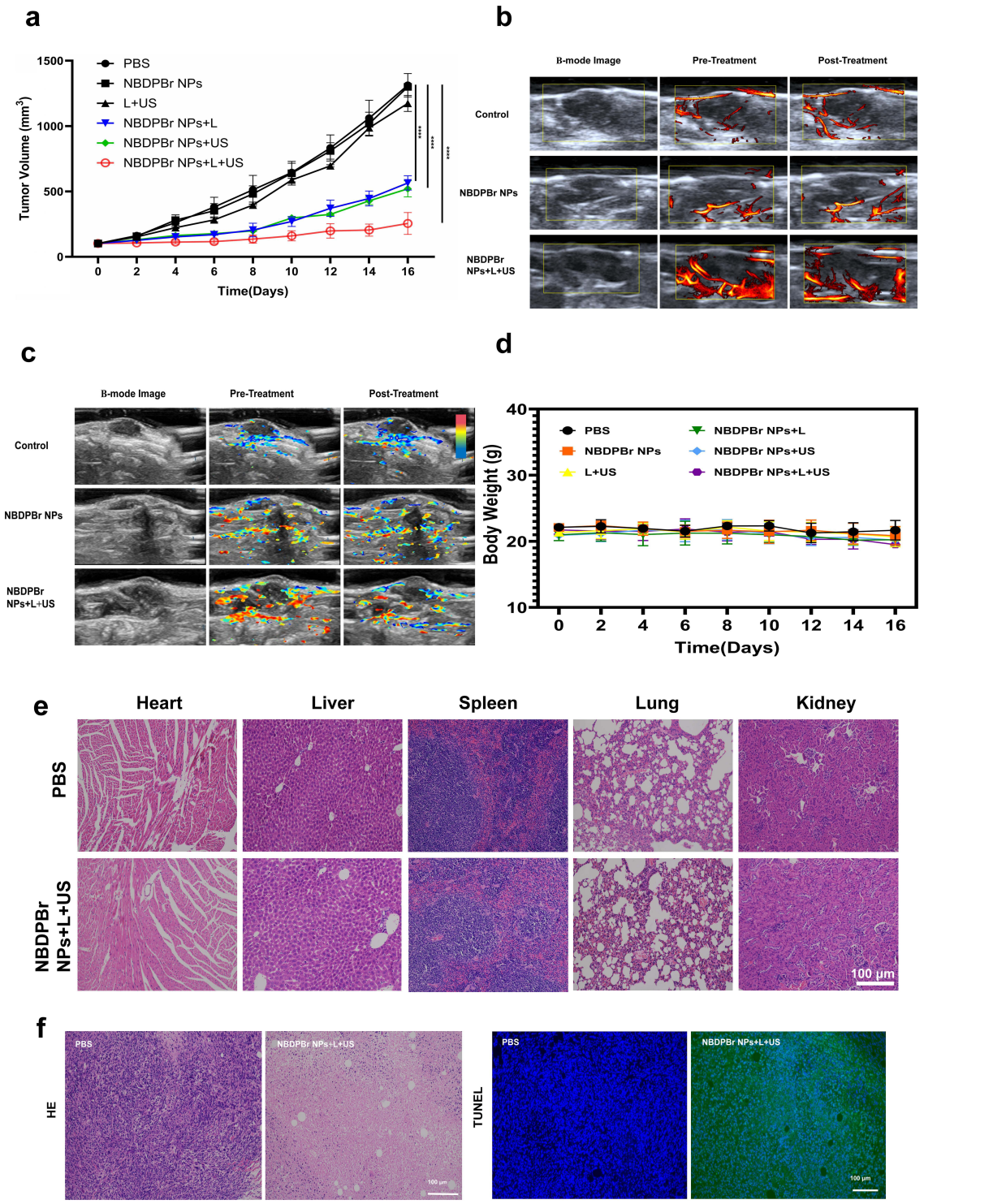

Figure 4 In vivo evaluation of NBDPBr NPs mediated combined PDT/SDT against TNBC. (**a**) Tumor growth curve of mice during a 16-day treatment period in different treatment groups (n=5), statistically significant differences were observed between the PBS group and the NBDPBr NPs + L, NBDPBr NPs + US, and NBDPBr NPs + L + US groups, **** indicating $P < 0.0001$; (**b**) Representative B-mode images (left column) and corresponding URM images before and after treatment are shown for the Control, NBDPBr NPs only, and NBDPBr NPs + L + US groups. The yellow coloured boxes in the URM images outline the regions of interest (ROIs) used for quantifying the vessel ratio, a metric reflecting microvascular density and perfusion; (**c**) PAI showing blood oxygen saturation (sO_2) in tumors before and after tumor treatment for the Control, NBDPBr NPs only, and NBDPBr NPs + L + US groups. The colorbar indicates sO_2 levels, with red representing higher and blue representing lower oxygen saturation. The images visualize the significant reduction in tumor oxygenation induced by the combined PDT/SDT treatment; (**d**) Body weight monitoring. Changes in body weight of tumor-bearing mice across different treatment groups over the 16-day experimental period (n = 6). No significant weight loss was observed in any group, indicating the absence of acute systemic toxicity; (**e**) HE staining of major organs (heart, liver, spleen, lungs, and kidneys) after different treatments. Scale bar = 100 μm; (**f**) Tumor section staining after different treatments. H&E staining reveals reduced cellularity and extensive necrotic areas in the combined treatment group (NBDPBr NPs + L + US). TUNEL staining shows a marked increase in apoptosis within tumors from the combined treatment group compared to controls. Scale bar = 100 μm.

https://doi.org/10.2147/IJN.S576927

Table 1 URM quantification of tumor microvascular density before and after treatment

Group	Vessel Ratio (%, Mean ± SD)		Change (Δ%, Mean ± SD)	P[1]
	Pre-Treatment[2]	Post-Treatment		
Control	7.42 ± 3.71	8.00 ± 3.65	+0.58 ± 0.55	0.102
NBDPBr NPs	6.98 ± 3.72	6.54 ± 3.88	−0.44 ± 0.90	0.397
NBDPBr NPs+L+US	11.16 ± 4.10	8.06 ± 3.65	−3.10 ± 1.14	0.027*

Notes: [1]Intra-group comparisons (pre- vs. post-treatment) were performed using paired t-test. *P < 0.05 indicates a statistically significant difference. [2]One-way ANOVA confirmed no statistically significant difference in baseline (pre-treatment) vessel ratio among the three groups (P = 0.075).

confirmed the comparability between the groups. After treatment, the vascular ratio of the control group and the NBDPBr NPs group increased slightly, but the comparison in the group was not statistically significant (P > 0.05). However, the combined treatment group showed a significant and continuous decline, with the average vascular ratio decreasing from (11.16 ±4.10%) pre-treatment to (8.06 ±3.65%) post-treatment (P < 0.05). This quantitative result confirms that only when NBDPBr NPs were activated by laser and ultrasound at the same time, significant tumor vascular destruction will occur, which is consistent with the observed strong anti-tumor effect.

PAI

Figure 4c shows that the blood oxygen saturation level of each group of tumor tissue is different. The oxygen saturation of the blank control group and the NBDPBr NPs group was stable and the change was very little. In contrast, the oxygen saturation of the combined treatment group (NBDPBr NPs + L + US) decreased significantly, indicating that the therapy has a significant effect on tumor hypoxia. In addition, the results show that combined treatment significantly reduces tumor hypoxia. Unlike the single injection of NBDPBr NPs, it achieves better treatment than single drugs through the combined treatment mode.

Table 2 summarizes the quantitative analysis of the average tumor sO_2 before and after treatment. Statistical analysis confirmed that there is no significant difference between the three groups of baselines sO_2 (P = 0.105), which ensures the comparability. After treatment, the sO_2 in the control group increased slightly, but there was no significant difference (from 57.26% to 58.53%, P = 0.102). Similarly, the NBDPBr NPs group only showed small and non-significant changes (from 57.19% to 58.40%, P = 0.397). On the contrary, the tumor sO_2 in the NBDPBr NPs + L + US group decreased significantly and substantially, from 70.09% of the baseline to 60.61% after treatment (P = 0.002). In addition, the inter-group comparison of treatment-induced changes (ΔsO_2) showed that the reduction in the combined treatment group was significantly greater than that of the control group and the only NBDPBr NPs group (P < 0.001 for both comparisons). These quantitative evidences strongly show that combined PDTSDT effectively aggravates tumor hypoxia, which is the key mechanism of its strong anti-tumor effect.

Table 2 PAI quantification of tumor sO_2 before and after treatment

Group	sO_2(%, Mean ± SD)		Change (ΔsO_2%, Mean ± SD)	P[1]
	Pre-Treatment[2]	Post-Treatment		
Control	57.26 ± 6.04	58.53 ± 5.45	+1.27 ± 1.41	0.102
NBDPBr NPs	57.19 ± 6.74	58.40 ± 6.39	+1.21 ± 1.53	0.397
NBDPBr NPs+L+US	70.09 ± 5.54	60.61 ± 6.47	−9.48 ± 1.52	0.002*

Notes: [1]Intra-group comparisons (pre- vs. post-treatment) were performed using paired t-test. *P < 0.05 indicates a statistically significant difference. [2]One-way ANOVA confirmed no statistically significant difference in baseline (pre-treatment) sO_2 among the three groups (P = 0.105). One-way ANOVA on the ΔsO_2 values showed a significant inter-group difference (P < 0.001). Tukey's post hoc test confirmed that the ΔsO_2 in the NBDPBr NPs + L + US group was significantly lower than that in both the Control (P < 0.001) and NBDPBr NPs (P < 0.001) groups.

https://doi.org/10.2147/IJN.S576927

Biosafety Evaluation

Throughout the experiment, mice in all groups maintained stable weight (Figure 4d) and exhibited normal behavior without signs of poisoning. No significant differences were observed between the treatment and control groups ($P>0.05$).

Histological analysis of key organs (heart, liver, spleen, lung, and kidney) in mice (Figure 4e) revealed no significant damage or inflammation, suggesting that NBDPBr NPs and photo-acoustic dynamic therapy are biologically safe and non-toxic.

Histological Examination

Figure 4f illustrates that H&E staining showed fewer tumor cells and large necrotic areas after combined therapy, indicating complete cancer cell elimination. TUNEL staining also revealed more apoptotic cells in the combined treatment group, highlighting the effectiveness of photo-acoustic synergy in targeting TNBC and significantly inhibiting tumor growth.

Discussion

PDT and SDT have recently become popular in the treatment of solid tumours due to their non-invasive nature and effective targeting capabilities.[11,12] Many photosensitizers also have acoustic sensitivity. Nanodevice-based drug delivery systems (NDDS) can improve therapeutic outcomes by enhancing tumour targeting and delivery depth.[13] This study uses NBDPBr NPs,[10] a novel nano-photonic sensitiser derived from a dual-brominated Aza-BODIPY dye. NBDPBr NPs show high oxygen quantum yield and photothermal conversion efficiency, as well as excellent photoacoustic imaging and biocompatibility. While our previous work characterized its high singlet oxygen quantum yield and photothermal conversion efficiency for phototherapy, the present study systematically expands its functionality by investigating its previously unexplored sonodynamic activity and establishing a combined PDT/SDT regimen. By leveraging the deep penetration of ultrasound to overcome the shallow light penetration in PDT, multimodal imaging is used to visualize the treatment, validating the effectiveness of the sensitizer in PDT/SDT therapy for TNBC.[6]

To address the inherent hydrophobicity of the NBDPBr dye and enable tumor-targeted delivery, we encapsulated it within amphiphilic polymer F-127 to form NBDPBr NPs. This amphiphilic copolymer forms a core-shell structure, providing a hydrophobic core for NBDPBr encapsulation and a hydrophilic poly(ethylene oxide) (PEO) shell that ensures aqueous solubility and colloidal stability primarily through steric hindrance.

Although the measured zeta potential was moderate (−5.45 mV), the primary stabilization mechanism for such non-ionic polymer-coated nanoparticles is steric rather than electrostatic. The practical stability of the formulation is demonstrated by its low polydispersity (PDI = 0.176) and the absence of aggregation or size change in an aqueous suspension over one week. The resulting uniform NBDPBr NPs (about 80 nm) improve solubility, stability and tumor accumulation through EPR effects, providing support for subsequent image-guided synergistic therapy.

When sensitizer NBDPBr NPs are exposed to laser and ultrasound at the same time, a large amount of ROS will be generated, which will lead to apoptosis of tumor cells and achieve effective PDT/SDT.

In vitro experiments showed that extending the irradiation time of laser and ultrasound significantly improves the level of ROS produced by NBDPBr NPs. The photoacoustic combined treatment group was obviously better than the single-mode treatment group, achieving 96.02% cell mortality in 4T1 breast cancer cells.

The superior anti-tumor effect observed in the combined PDT/SDT group can be attributed to the multi-level synergy mechanism. At the molecular level, the dibrominated Aza-BODIPY structure of NBDPBr promotes effective intersystem crossing (ISC) through the heavy atomic effect,[9,10] enables the triple state to be fully filled, which is crucial for the generation of $^1O_2$.[14] At the physical level, ultrasound irradiation enhances the distribution and cell uptake of nanoparticles in tumors through sound flow and cavitation effects.[15,16] In addition, ultrasound-induced sonoporation can temporarily increase the permeability of cell membranes, thus promoting nanoparticles and externally generated ROS into the cell, thus reducing the threshold of oxidative damage.[6,15]

We proposed a two-stage activation mechanism: laser pre-irradiation excites the sensitizer and produces the initial $^1O_2$ burst, and the subsequent ultrasound irradiation further amplifies the generation of ROS by activating more sensitizer

molecules and promoting their physical transfer to cells. This synergy may be the reason why we have observed that the level of ROS and cytotoxicity significantly exceed that of using any method alone.

In addition, as previously reported,[10] the inherent photothermal properties of NBDPBr NPs may contribute to the overall therapeutic effect. The localized hyperthermia caused by laser irradiation can directly damage tumor cells and blood vessels, while enhancing the therapeutic effect of PDT/SDT by increasing membrane permeability and inhibiting cell repair process.[15] Therefore, the final therapeutic effect may be the result of the synergy of PDT, SDT and photothermal therapy (PTT).

Consistent with the results of in vitro experiments, in vivo experiments show that in the syngeneic TNBC mouse model, the combined treatment mediated by NBDPBr NPs can effectively inhibit tumor growth, and no obvious systemic toxicity has been observed. Histological analysis by H&E and TUNEL staining confirmed that the tumor cells in the combined treatment group had extensive necrosis and apoptosis, which further confirmed its therapeutic effect.

Photoacoustic dynamic therapy (SPDT), combining SDT and PDT, is a promising anti-tumor approach.[4] Liu et al[17] developed a nanomaterial, PARN, using rose red and an amphiphilic peptide, which showed over 95% tumor growth inhibition in mice, outperforming individual SDT or PDT. This treatment increased ROS production and triggered apoptosis and necrosis in tumor cells without harming vital organs. Additionally, Zhao Ruimei[18] demonstrated that oxygen-producing cyanobacteria enhance SPDT's antitumor effects, highlighting its potential as a safe, non-invasive breast cancer treatment.

The development of tumors usually involves abnormal angiogenesis and hypoxic environment,[19] which enhances its aggressiveness and metastaticity.[20] This study uses URM and PAI to monitor the PDT/SDT treatment of TNBC and evaluate the risk of blood supply, metabolism and metastasis of tumors. URM provides micron-level resolution by tracking contrast agent microparticles in blood vessels, surpassing the limitations of traditional ultrasound. It can clearly show the changes of tumor microvessels and conduct quantitative hemodynamic analysis,[7] combining the ability of deep tissue penetration[21] and the real-time, non-invasive and repeatability characteristics of ultrasound. PAI can identify endogenous light absorbers,[22] such as hemoglobin,[23] measure oxygen saturation (sO_2) of tumor tissue, and visualize vascular structure and blood flow. These characteristics provide insights for understanding the tumor microenvironment and help guide treatment. URM imaging shows that the density of tumor microvessels decreases and blood flow weakens after combined treatment, which may be due to the damage of tumor blood vessels by photoacoustic effects,[24] resulting in vascular occlusion or damage, thus reducing blood supply. The results of PAI also show that the level of sO_2 decreased after treatment, indicating the increase of hypoxia and the enhancement of apoptosis induced by ROS.[25] This observed decrease in the level of tumor oxygenation, although it seems to be contradictory to the oxygen-dependent Type II photodynamic process, it can be explained mechanically, and in fact it also highlights the therapeutic cascade response.

At first, the abundant oxygen in the tumor microenvironment supported the efficient generation of $^1O_2$ through the Type II pathway after NBDPBr NPs was activated. The outbreak of ROS, especially $^1O_2$, directly damages tumor cells and, crucially, targets tumor blood vessels. As confirmed by URM results, the density of microvessels is reduced.[24] The resulting vascular damage will damage blood perfusion and oxygen delivery, resulting in a decrease in sO_2 measured by PAI. Therefore, the initial oxygen-dependent ROS generation started a self-amplifying cascade reaction, eventually causing a hypoxic environment in the tumor.

This may reflects a therapeutic cascade: in the process of $^1O_2$ generation driven by PDT, the initial oxygen is consumed; the resulting ROS then damages the tumor blood vessels (as shown in URM), affecting perfusion and oxygen delivery, and ultimately leading to increased tumor hypoxia. This induced hypoxia is not a treatment failure, but a successful biomarker of blood vessel destruction, and may further enhance SDT with less oxygen dependence.

Importantly, treatment-induced hypoxia itself may trigger an adaptive response. Tumor cells improve oxygenation and adapt to hypoxia by promoting the formation of new blood vessels. With the growth of the tumor, the level of sO_2 will fluctuate. As previously reported,[26] after this compensatory vascular proliferation, sO_2 may rebound periodically. This highlights the dynamic characteristics of the tumor microenvironment after treatment and emphasizes the value of our dual-modal imaging platform (URM/PAI), which can not only capture the initial treatment damage, but also capture potential subsequent adaptive changes, thus providing a basis for repeated or combined treatment plans.

 https://doi.org/10.2147/IJN.S576927

This dual-mode imaging technology breaks through the traditional limitations of depth and contrast, and can evaluate in detail from vascular structure to blood oxygen changes. It can monitor vascular blockage, blood flow changes and oxygen metabolism in real time during treatment, and provide multimodal imaging guidance for the accurate diagnosis and treatment of TNBC.

The treatment of TNBC is quite challenging because of the lack of molecular markers for targeted drugs, and conventional cytotoxic therapies have side effects and are prone to drug resistance. However, photoacoustic synergistic therapy provides a precise and non-invasive alternative. This study combines visualization and intervention through nanoengineering means, showing encouraging results, which may open up a new way for the treatment of TNBC with limited choices.

This research has several limitations, which indicate the direction for future research. First of all, although 4T1 cells provide a standard TNBC model, its efficacy should be verified in human TNBC cell lines and xenotransplant models derived from patients to better simulate the heterogeneity of human tumors.[27] Secondly, although the sample size (n=5 per group) is consistent with standard preclinical practice and the observed effect sizes were substantial, the statistical power remains limited. Future investigations involving larger animal cohorts and multi-center validation are warranted to confirm these findings and facilitate clinical translation. Thirdly, although excellent biosafety has been observed, detailed pharmacokinetics, biological distribution and long-term toxicological studies are still needed to comprehensively evaluate the conversion potential of the nanoplatform. Finally, although we focus on the direct cytotoxicity and anti-angiogenesis, the impact of this therapy on the tumor immune microenvironment deserves further study, because it may open up a new path for the combined application with immunotherapy.

Conclusion

In summary, this study proves that the novel Aza-BODIPY-based nanophotosensitizer NBDPBr NPs can effectively inhibit the growth of TNBC through synergistic PDT/SDT, while showing good biocompatibility. The integration of URM and PAI offers a valuable multimodal imaging platform for real-time treatment monitoring, which can capture changes in blood vessels and oxygenation. These findings provide promising preliminary preclinical concept verification for targeted and non-invasive treatment strategies for TNBC.

Data Sharing Statement

All raw data are available upon request.

Ethics Statement

Ethical approval was granted by Nanjing Medical University Experimental Animal Ethics Committee.

Acknowledgments

This work was supported by grants from the Scientific Research Program of Jiangsu Commission of Health (grant number: ZD2021014); and International Science and Technology Cooperation Program of the National Natural Science Foundation of China (grant number: 62120106002); and Jiangsu Cancer Hospital Science and Technology Development Fund Project (grant number: QZLC202414). We gratefully acknowledge the technical assistance provided by the core facilities of the Affiliated Cancer Hospital of Nanjing Medical University and Nanjing Tech University.

Author Contributions

All authors made a significant contribution to the work reported, whether that is in the conception, study design, execution, acquisition of data, analysis and interpretation, or in all these areas; took part in drafting, revising or critically reviewing the article; gave final approval of the version to be published; have agreed on the journal to which the article has been submitted; and agree to be accountable for all aspects of the work.

Funding

This study was supported by Scientific Research Program of Jiangsu Commission of Health (grant number: ZD2021014); and International Science and Technology Cooperation Program of the National Natural Science Foundation of China (grant number: 62120106002); and Jiangsu Cancer Hospital Science and Technology Development Fund Project (grant number: QZLC202414).

Disclosure

The authors have no conflict of interest.

References

1. Bray F, Laversanne M, Sung H, et al. Global cancer statistics 2022: GLOBOCAN estimates of incidence and mortality worldwide for 36 cancers in 185 countries. *CA Cancer J Clin*. 2024;74(3):229–263. doi:10.3322/caac.21834
2. Bareche Y, Venet D, Ignatiadis M, et al. Unravelling triple-negative breast cancer molecular heterogeneity using an integrative multiomic analysis. *Ann Oncol*. 2018;29(4):895–902. doi:10.1093/annonc/mdy024
3. Dong H, Wu R, Liu J, et al. Progress in the study of photodynamic therapy for tumors. *J China Pharm Univ*. 2016;47(3):377–387.
4. Zhu L, Ren J, Zhou Z. Advances in combined tumor therapy based on acoustic dynamic therapy. *J Med Res*. 2024;53:25–28,68.
5. Chen L, Huang J, Li X, et al. Progress of nanomaterials in photodynamic therapy against tumor. *Front Bioeng Biotechnol*. 2022;10:920162. doi:10.3389/fbioe.2022.920162
6. Zhang Z, Yang D, Zhang X, et al. Research progress on sonotherapism. *J Clin Ultrasound Med*. 2021;23:611–614. doi:10.16245/j.cnki.issn1008-6978.2021.08.009
7. Xia S, Hua Q, Song Y, et al. Super-resolution ultrasound imaging of intranodal lymphatic sinuses for predicting sentinel lymph node metastasis in breast cancer: a preliminary study. *Eur Radiol*. 2025;35(10):6079–6088. doi:10.1007/s00330-025-11520-5
8. Attia ABE, Balasundaram G, Moothanchery M, et al. A review of clinical photoacoustic imaging: current and future trends. *Photoacoustics*. 2019;16:100144. doi:10.1016/j.pacs.2019.100144
9. Hu C. Construction and performance study of a novel near-infrared Aza-BODIPY optical diagnostic agent [dissertation]. Beijing University of Chemical Technology; 2023. doi:10.26939/d.cnki.gbhgu.2023.000609.
10. Wang L, Mei A, Li N, et al. Aza-BODIPY dye with unexpected bromination and high singlet oxygen quantum yield for photoacoustic imaging-guided synergetic photodynamic/photothermal therapy. *Chin Chem Lett*. 2024;35(6):108974. doi:10.1016/j.cclet.2023.108974
11. Guo L, Wang Q, Liu J, et al. Innovative strategies for enhanced tumor photodynamic therapy. *J Mater Chem B*. 2021;9(36):7347–7370. doi:10.1039/D1TB01466H
12. Zhang P, Xiao Y, Sun X, et al. Cancer nanomedicine toward clinical translation: obstacles, opportunities, and future prospects. *Med*. 2023;4(3):147–167. doi:10.1016/j.medj.2022.12.001
13. Zheng Y, Ye J, Li Z, et al. Recent progress in sono-photodynamic cancer therapy: from developed new sensitizers to nanotechnology-based efficacy-enhancing strategies. *Acta Pharm Sin B*. 2021;11(8):2197–2219. doi:10.1016/j.apsb.2020.12.016
14. Li X, Yang M, Peng Q. Research progress on photosensitizers in photodynamic therapy. *Chem Res*. 2025;36(2):168–179. doi:10.14002/j.hxya.2025.02.010
15. He Z, Du J, Miao Y, et al. Recent developments of inorganic nanosensitizers for sonodynamic therapy. *Adv Healthc Mater*. 2023;12(22):e2300234. doi:10.1002/adhm.202300234
16. Li D, Lu X, Zhang W. Advances in the study of sonodynamic therapy combined with immunotherapy in cancer treatment. *Mod Oncol Med*. 2024;1–5.
17. Liu Z, Li J, Jiang Y, et al. Multifunctional nanocapsules on a seesaw balancing sonodynamic and photodynamic therapies against superficial malignant tumors by effective immune-enhancement. *Biomaterials*. 2019;218:119251. doi:10.1016/j.biomaterials.2019.119251
18. Zhao R. In situ oxygen production by cyanobacteria and its photoacoustic dynamic therapy for breast cancer [dissertation]. Nanhua University; 2022. doi:10.27234/d.cnki.gnhuu.2022.000844.
19. Huang K, Zhang L, Lin L. Progress in breast photoacoustic imaging. *Chin J Laser*. 2024;51:37–49.
20. Madu CO, Wang S, Madu CO, et al. Angiogenesis in breast cancer progression, diagnosis, and treatment. *J Cancer*. 2020;11(15):4474–4494. doi:10.7150/jca.44313
21. Chu B, Chen Z, Shi H, et al. Fluorescence, ultrasonic and photoacoustic imaging for analysis and diagnosis of diseases. *Chem Commun*. 2023;59(17):2399–2412. doi:10.1039/D2CC06654H
22. Diot G, Metz S, Noske A, et al. Multispectral optoacoustic tomography (MSOT) of human breast cancer. *Clin Cancer Res*. 2017;23(22):6912–6922. doi:10.1158/1078-0432.CCR-16-3200
23. Li M, Tang Y, Yao J, et al. Photoacoustic tomography of blood oxygenation: a mini review. *Photoacoustics*. 2018;10:65–73. doi:10.1016/j.pacs.2018.05.001
24. Niu H, Shi L, Yu Y, et al. Antitumor mechanism of photodynamic therapy and research progress in esophageal cancer. *Esophageal Dis*. 2023;5(2):87–91.
25. Reina-Campos M, Moscat J, Diaz-Meco M, et al. Metabolism shapes the tumor microenvironment. *Curr Opin Cell Biol*. 2017;48:47–53. doi:10.1016/j.ceb.2017.05.006
26. Fang Z, Wang C, Yang J, et al. Oxyhaemoglobin saturation NIR-IIb imaging for assessing cancer metabolism and predicting the response to immunotherapy. *Nat Nanotechnol*. 2024;19(1):124–130. doi:10.1038/s41565-023-01501-4
27. Guillen KP, Fujita M, Butterfield AJ, et al. A human breast cancer-derived xenograft and organoid platform for drug discovery and precision oncology. *Nat Cancer*. 2022;3(2):232–250. doi:10.1038/s43018-022-00337-6